Article

r-Process elements from magnetorotational hypernovae

https://doi.org/10.1038/s41586-021-03611-2

Received: 5 November 2020

Accepted: 4 May 2021

Published online: 7 July 2021

Check for updates

D. Yong[1,2]✉, C. Kobayashi[2,3], G. S. Da Costa[1,2], M. S. Bessell[1], A. Chiti[4], A. Frebel[4], K. Lind[5], A. D. Mackey[1,2], T. Nordlander[1,2], M. Asplund[6], A. R. Casey[2,7], A. F. Marino[8], S. J. Murphy[1,9] & B. P. Schmidt[1]

Neutron-star mergers were recently confirmed as sites of rapid-neutron-capture (r-process) nucleosynthesis[1–3]. However, in Galactic chemical evolution models, neutron-star mergers alone cannot reproduce the observed element abundance patterns of extremely metal-poor stars, which indicates the existence of other sites of r-process nucleosynthesis[4–6]. These sites may be investigated by studying the element abundance patterns of chemically primitive stars in the halo of the Milky Way, because these objects retain the nucleosynthetic signatures of the earliest generation of stars[7–13]. Here we report the element abundance pattern of the extremely metal-poor star SMSS J200322.54−114203.3. We observe a large enhancement in r-process elements, with very low overall metallicity. The element abundance pattern is well matched by the yields of a single 25-solar-mass magnetorotational hypernova. Such a hypernova could produce not only the r-process elements, but also light elements during stellar evolution, and iron-peak elements during explosive nuclear burning. Hypernovae are often associated with long-duration γ-ray bursts in the nearby Universe[8]. This connection indicates that similar explosions of fast-spinning strongly magnetized stars occurred during the earliest epochs of star formation in our Galaxy.

The SkyMapper telescope has surveyed the southern sky[14] and identified thousands of chemically primitive stars[15], including the red giant SMSS J200322.54−114203.3 (hereafter SMSS 2003−1142). The metallicity of this star is [Fe/H] = −3.5, determined from analysis of the high-resolution spectrum (see below and Methods). (Here $[A/B] \equiv \log(N_A/N_B)_{star} - \log(N_A/N_B)_{\odot}$, where N_A/N_B is the number ratio of atoms of elements A and B, the subscript ⊙ refers to the solar value and $\log\varepsilon(A) \equiv \log(N_A/N_H) + 12.00$.) It contains a very low abundance of heavy elements, or metals, with an iron-to-hydrogen ratio 3,000 times lower than that for the Sun. We therefore postulate that all the elements in SMSS 2003−1142, from carbon to the r-process element uranium, were probably produced by a single zero-metallicity progenitor star. Of particular interest is the fact that SMSS 2003−1142 is one of a small number of extremely metal-poor stars that exhibit large enhancements in the abundances of r-process elements.

We obtained high-resolution spectroscopic observations of SMSS 2003−1142 to conduct a detailed chemical abundance analysis (Table 1) and infer the properties of its progenitor (Methods). We find a high nitrogen-to-iron abundance ratio ([N/Fe] = +1.07) relative to the carbon abundance ([C/Fe] < 0.07; with minimal correction for evolutionary mixing; Methods), which is strongly suggestive of a rapidly rotating progenitor star[16]. Furthermore, the high zinc abundance ([Zn/Fe] = +0.72) can be explained only as originating from supernovae with large explosion energies[8]. For all other elements between carbon and zinc, the abundance pattern of SMSS 2003−1142 lies within the distribution of abundance patterns exhibited by other extremely metal-poor stars ([Fe/H] < −3) and is probably due to a single enrichment event from a zero-metallicity progenitor.

We also measured the relative abundances (or upper limits) for 28 neutron-capture elements from strontium (atomic number $Z = 38$) to uranium ($Z = 92$). For all neutron-capture elements, the abundance ratios normalized to iron ([X/Fe]) are higher than the solar ratio. Among the known stars with large enhancements in r-process-element abundance, that is, those with [Eu/Fe] > +1.0, SMSS 2003−1142 is the most iron-poor object by a factor of about two. We plot the r-process-element abundances in Fig. 1 and compare the data to the scaled solar r-process distribution. For the elements from barium ($Z = 56$) to thulium ($Z = 69$), SMSS 2003−1142 exhibits the scaled solar r-process pattern that is also characteristic of r-process-enhanced stars[17]. For lighter ($Z < 56$) and heavier ($Z > 69$) elements, SMSS 2003−1142 exhibits lower and higher average abundances, respectively, when compared to the scaled solar r-process distribution. Compared to other known r-process-enhanced stars, SMSS 2003−1142 has the highest [X/Fe] abundance ratios for zinc, barium, europium and thorium, further highlighting the unusual nature of this star[18] (Methods).

[1]Research School of Astronomy and Astrophysics, Australian National University, Canberra, Australian Capital Territory, Australia. [2]ARC Centre of Excellence for All Sky Astrophysics in 3 Dimensions (ASTRO 3D), Canberra, Australian Capital Territory, Australia. [3]Centre for Astrophysics Research, Department of Physics, Astronomy and Mathematics, University of Hertfordshire, Hatfield, UK. [4]Department of Physics and Kavli Institute for Astrophysics and Space Research, Massachusetts Institute of Technology, Cambridge, MA, USA. [5]Department of Astronomy, Stockholm University, AlbaNova University Center, Stockholm, Sweden. [6]Max Planck Institute for Astrophysics, Garching, Germany. [7]School of Physics and Astronomy, Monash University, Melbourne, Victoria, Australia. [8]Istituto Nazionale di Astrofisica - Osservatorio Astronomico di Arcetri, Florence, Italy. [9]School of Science, The University of New South Wales, Canberra, Australian Capital Territory, Australia. ✉e-mail: david.yong@anu.edu.au

Table 1 | Chemical abundances of SMSS 2003–1142

Species	Z	logε(X)	N_{lines}	s.e.m.	[X/Fe]	Total error
C (CH)	6	<4.93			<0.07	0.30
N (NH)	7	5.33			1.07	0.30
Na I	11	2.80	2	0.09	0.13	0.11
Mg I	12	4.26	7	0.03	0.23	0.07
Al I	13	1.94	1		−0.94	0.16
Si I	14	4.27	1		0.33	0.17
Ca I	20	3.11	7	0.02	0.34	0.08
Sc II	21	0.09	1		0.37	0.19
Ti I	22	1.83	1		0.45	0.17
Ti II	22	1.77	17	0.05	0.26	0.12
Cr I	24	1.76	5	0.07	−0.31	0.10
Mn I	25	1.27	3	0.04	−0.59	0.10
Fe I	26	3.93	91	0.02	−3.57	0.11
Fe II	26	4.07	6	0.06	−3.43	0.13
Co I	27	1.78	3	0.08	0.36	0.11
Ni I	28	2.90	3	0.07	0.25	0.09
Cu I	29	<1.30	1		<0.68	0.16
Zn I	30	1.71	1		0.72	0.16
Sr II	38	0.20	2	0.02	0.76	0.17
Y II	39	−0.67	7	0.03	0.55	0.09
Zr II	40	−0.05	12	0.02	0.80	0.07
Mo I	42	−0.48	1		1.21	0.16
Ru I	44	−0.10	2	0.04	1.72	0.12
Rh II	45	<−0.78	1		<1.74	0.16
Pd I	46	<−0.72	1		<1.28	0.16
Ag I	47	<−1.71	1		<0.92	0.16
Ba II	56	−0.10	4	0.03	1.15	0.11
La II	57	−1.03	7	0.02	1.30	0.09
Ce II	58	−0.80	3	0.08	1.05	0.11
Pr II	59	−1.18	1		1.53	0.17
Nd II	60	−0.56	8	0.03	1.45	0.09
Sm II	62	−0.79	4	0.03	1.68	0.10
Eu II	63	−1.21	4	0.02	1.70	0.10
Gd II	64	−0.65	6	0.03	1.71	0.09
Tb II	65	−1.32	1		1.81	0.16
Dy II	66	−0.56	14	0.02	1.77	0.07
Ho II	67	−1.31	2	0.01	1.64	0.12
Er II	68	−0.80	5	0.03	1.71	0.09
Tm II	69	−1.53	3	0.09	1.80	0.11
Yb II	70	−0.60	1		1.99	0.16
Lu II	71	−0.94	1		2.39	0.16
Hf II	72	−1.12	1		1.46	0.16
Os I	76	0.00	1		2.17	0.16
Pb I	82	<−0.10	1		<1.72	0.16
Th II	90	−1.31	2	0.09	2.10	0.12
U II	92	−1.91	1		2.06	0.16

N_{lines}, number of lines used to analyse the given species; s.e.m., standard error of the mean.

In Fig. 2, we compare the abundance pattern of SMSS 2003–1142 with nucleosynthesis yields of a magnetorotational hypernova from a zero-metallicity $25M_{\odot}$ star to learn more about the enrichment source. The observed abundance pattern at $Z < 31$ is well reproduced by energetic (more than 10^{52} erg) core-collapse supernovae from massive stars (mass $M > 25M_{\odot}$)—that is, hypernovae[8,13]. By contrast, the pattern at $Z > 37$ requires the r-process, as in magnetorotational supernovae[4,19,20]. We therefore propose magnetorotational hypernovae as the enrichment source, assuming that the hypernova-type event (that is, an energetic supernova producing $0.017M_{\odot}$ of iron) is associated with an ejection of neutron-rich matter (Methods). The mass of the neutron-rich ejecta ($0.00035M_{\odot}$) is obtained by matching the observed [Eu/Fe] ratio with theoretical yields. This model reproduces many of the key features of the observed abundance pattern from carbon to uranium, including the normal [C/Fe] ratio, normal [α/Fe] ratio (where α refers to the average of Mg, Si and Ca), low [Mn/Fe] ratio, high [(Co,Zn)/Fe] ratio, enhancement of the first and second peaks of neutron-capture elements, low [Pb/Fe] ratio and high [(Th,U)/Fe] ratio. Around the second peak (barium to neodymium, inclusive), the model predicts lower abundance ratios than observed, but the agreement could be improved by fine-tuning the model parameters (Methods). The observed enhancements of nitrogen and sodium are not produced because of the lack of stellar rotation in the pre-supernova model. Scandium and titanium are known to be underproduced in one-dimensional supernova models (and are usually excluded from modelling of extremely metal-poor stars)[12]. The low [Mn/Fe] ratio provides a constraint on the material from type Ia supernovae[21]; for SMSS 2003–1142, there is no evidence for any contribution from type Ia supernovae, and the prediction of our preferred model is consistent with the observed ratio. Although the abundance pattern from carbon to iron could be reproduced by normal-energy supernova models, the high [X/Fe] ratios for cobalt and zinc are strongly suggestive of a high explosion energy, as in hypernovae.

Neutron-star mergers were first posited around 40 years ago as a site for r-process nucleosynthesis[22]. This theory was recently confirmed by direct observations of an astronomical transient kilonova (AT2017gfo)[2] and a short γ-ray burst[23] following the gravitational-wave detection event GW170817. Hence, Fig. 2 includes a neutron-star merger as an alternative model[24]. We assume that the neutron-star merger occurs in an interstellar medium that has already been enriched by core-collapse supernovae up to [Fe/H] ≈ −3.5 (Methods). In this model[18], the metallicity of [Fe/H] ≈ −3.5 is reached roughly 60 Myr after the onset of galaxy formation. Although the general abundance pattern of SMSS 2003–1142 is matched, this model does not reproduce some of the key features. The predicted [α/Fe] ratio is about 0.35 dex higher than the observed value. Also, the [(Co,Zn)/Fe] ratios are about 0.6 dex lower than for our preferred supernova model, which underscores the importance of a hypernova contribution. Further, the predicted thorium and uranium abundances for the neutron-star merger model are inconsistent with the observations. On the other hand, the predicted abundances around the second peak (barium to neodymium, inclusive) are higher than those for the magnetorotational supernova yields[20]. However, the mismatches of the magnetorotational hypernova model could be resolved by nuclear fissions and/or future self-consistent simulations (Methods); no special significance should be assigned to this difference.

The roughly 60-Myr iron-enrichment timescale in the alternative model is much shorter than that expected for neutron-star mergers, so, at this epoch, the rate of neutron-star mergers is extremely low[18]. We regard this as further evidence that the neutron-star merger hypothesis is less satisfactory than our magnetorotational hypernova scenario. Not only does our preferred model provide a better fit to the data, it also involves only a single enrichment event, in contrast to the neutron-star merger scenario, which requires multiple generations of star formation. Given the low metallicity of SMSS 2003–1142, a neutron-star merger origin would require new constraints on the formation, evolution and merger timescale for such objects, because the merger event must have occurred very shortly after the onset of galaxy formation. Although it is possible that more than one star contributed to the enrichment of SMSS 2003–1142, this is not required to explain the data. In summary, our analysis of SMSS 2003–1142 reveals evidence for r-process

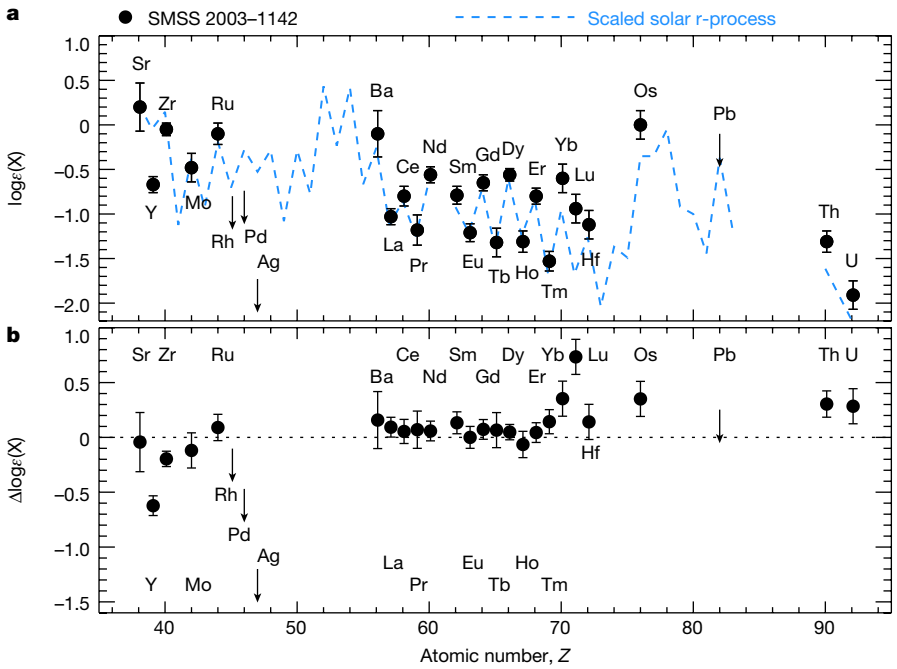

Fig. 1 | r-Process element abundance pattern of SMSS 2003–1142. a, The abundance pattern for SMSS 2003–1142 (black data) compared to the scaled solar r-process distribution (normalized to the europium abundance; blue dashed line). **b**, The abundance differences (SMSS 2003–1142 minus solar r-process). Arrows denote upper limits. The error bars are 1σ estimates of the uncertainties in our measurements (Methods).

nucleosynthesis from magnetorotational hypernovae, which may have occurred before the first neutron-star mergers, in the earliest stages of galaxy formation.

In Galactic chemical evolution models, the contribution from hypernovae is very important for explaining the behaviour of the abundance patterns of elements such as zinc and cobalt[21]. Galactic chemical evolution models cannot reproduce the observed r-process-element abundance patterns using neutron-star mergers alone, and other r-process sites such as magnetorotational supernovae have been supported[5,18]. However, the connection between hypernovae and magnetorotational supernovae, namely, the explosion mechanism, is uncertain. Numerical simulations show that neutrino-driven convection[25,26] can result in the explosion of stars with $M < 25M_{\odot}$, which leave behind a neutron star. It is not yet known how more massive stars ($M > 25M_{\odot}$), which leave behind a black hole remnant, explode. However, in the nearby Universe, the explosions of such massive stars have been observed as broad-lined

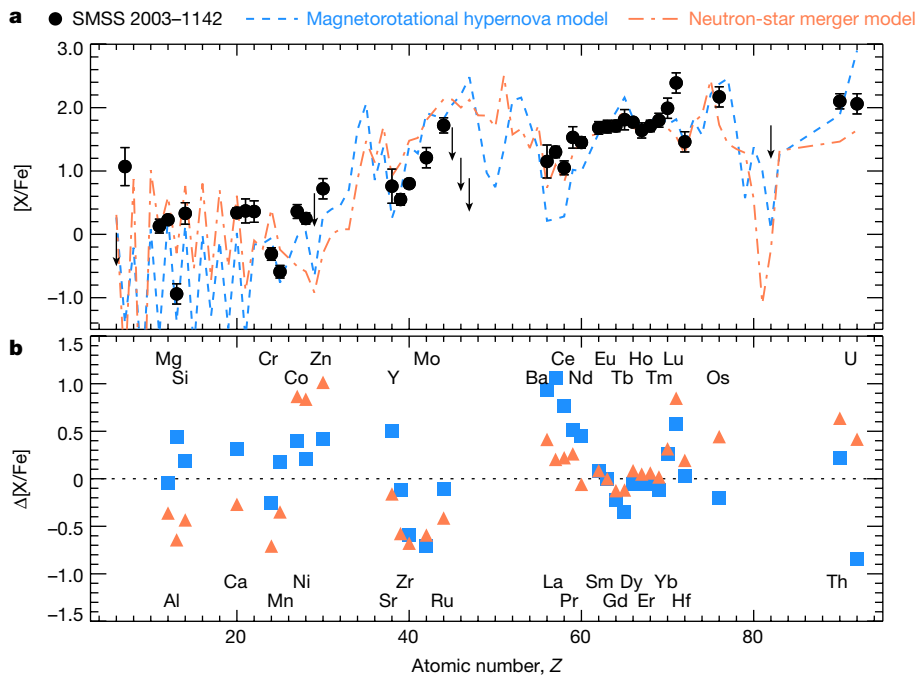

Fig. 2 | Comparison of models and data. a, Element abundance pattern for SMSS 2003–1142 (black data; arrows denote upper limits) compared with the $25M_{\odot}$ magnetorotational hypernova model (blue dashed line) and neutron-star merger model (red dot–dashed line). **b**, Differences (SMSS 2003–1142 minus magnetorotational hypernova model (blue squares) or neutron-star merger model (red triangles)), excluding abundance limits and the elements nitrogen, sodium, scandium and titanium (Methods). The root-mean-square values are 0.44 dex and 0.47 dex for the magnetorotational hypernova and neutron-star merger models, respectively. For our preferred set of elements ($Z < 56$ and $Z > 60$; Methods), the root-mean-square values are 0.34 dex and 0.50 dex for the magnetorotational hypernova and neutron-star merger models, respectively. The error bars are estimates of the 1σ uncertainties in our measurements (Methods).

type Ic supernovae and are often associated with long-duration γ-ray bursts, which implies that stellar rotation and/or magnetic fields produce a jet that ejects iron-rich matter from near the central black hole. Collapsars[27] and magnetars[28] have been proposed as models of the central engine of long-duration γ-ray bursts. Our magnetorotational hypernova model assumes a similar mechanism. This class of stellar explosions may be more important in the early Universe, because in primordial stars the lack of stellar winds results in substantially less mass loss and so faster rotation is expected. Magnetic fields should grow substantially at the formation sites of some of the first stars. The discovery and analysis of SMSS 2003–1142 reveals magnetorotational hypernovae as a source of r-process elements during the earliest epochs of star formation in the Galaxy, and will hopefully stimulate further theoretical study of these energetic events.

Online content

Any methods, additional references, Nature Research reporting summaries, source data, extended data, supplementary information, acknowledgements, peer review information; details of author contributions and competing interests; and statements of data and code availability are available at https://doi.org/10.1038/s41586-021-03611-2.

1. Ji, A. P., Frebel, A., Chiti, A. & Simon, J. D. r-Process enrichment from a single event in an ancient dwarf galaxy. *Nature* **531**, 610–613 (2016).
2. Pian, E. et al. Spectroscopic identification of r-process nucleosynthesis in a double neutron-star merger. *Nature* **551**, 67–70 (2017).
3. Kasen, D., Metzger, B., Barnes, J., Quataert, E. & Ramirez-Ruiz, E. Origin of the heavy elements in binary neutron-star mergers from a gravitational-wave event. *Nature* **551**, 80–84 (2017).
4. Winteler, C. et al. Magnetorotationally driven supernovae as the origin of early galaxy r-process elements? *Astrophys. J.* **750**, L22 (2012).
5. Haynes, C. J. & Kobayashi, C. Galactic simulations of r-process elemental abundances. *Mon. Not. R. Astron. Soc.* **483**, 5123–5134 (2019).
6. Siegel, D. M., Barnes, J. & Metzger, B. D. Collapsars as a major source of r-process elements. *Nature* **569**, 241–244 (2019).
7. Umeda, H. & Nomoto, K. First-generation black-hole-forming supernovae and the metal abundance pattern of a very iron-poor star. *Nature* **422**, 871–873 (2003).
8. Nomoto, K., Kobayashi, C. & Tominaga, N. Nucleosynthesis in stars and the chemical enrichment of galaxies. *Annu. Rev. Astron. Astrophys.* **51**, 457–509 (2013).
9. Frebel, A. & Norris, J. E. Near-field cosmology with extremely metal-poor stars. *Annu. Rev. Astron. Astrophys.* **53**, 631–688 (2015).
10. Bessell, M. S. et al. Nucleosynthesis in a primordial supernova: carbon and oxygen abundances in SMSS J031300.36–670839.3. *Astrophys. J.* **806**, L16 (2015).
11. Nordlander, T. et al. 3D NLTE analysis of the most iron-deficient star, SMSS0313–6708. *Astron. Astrophys.* **597**, A6 (2017).
12. Ishigaki, M. N. et al. The initial mass function of the first stars inferred from extremely metal-poor stars. *Astrophys. J.* **857**, 46 (2018).
13. Ezzeddine, R. et al. Evidence for an aspherical population III supernova explosion inferred from the hyper-metal-poor star HE 1327–2326. *Astrophys. J.* **876**, 97 (2019).
14. Wolf, C. et al. SkyMapper southern survey: first data release (DR1). *Publ. Astron. Soc. Aust.* **35**, e010 (2018).
15. Da Costa, G. S. et al. The SkyMapper DR1.1 search for extremely metal-poor stars. *Mon. Not. R. Astron. Soc.* **489**, 5900–5918 (2019).
16. Maeder, A. & Meynet, G. Rotating massive stars: from first stars to gamma ray bursts. *Rev. Mod. Phys.* **84**, 25–63 (2012).
17. Sneden, C. S., Cowan, J. J. & Gallino, R. Neutron-capture elements in the early galaxy. *Annu. Rev. Astron. Astrophys.* **46**, 241–288 (2008).
18. Kobayashi, C., Karakas, A. I. & Lugaro, M. The origin of elements from carbon to uranium. *Astrophys. J.* **900**, 179 (2020).
19. Symbalisty, E. M. D. Magnetorotational iron core collapse. *Astrophys. J.* **285**, 729–746 (1984).
20. Nishimura, N., Takiwaki, T. & Thielemann, F.-K. The r-process nucleosynthesis in the various jet-like explosions of magnetorotational core-collapse supernovae. *Astrophys. J.* **810**, 109 (2015).
21. Kobayashi, C. et al. Galactic chemical evolution: carbon through zinc. *Astrophys. J.* **653**, 1145–1171 (2006).
22. Lattimer, J. M. & Schramm, D. N. Black-hole-neutron-star collisions. *Astrophys. J.* **192**, L145–L147 (1974).
23. Abbott, B. P. et al. GW170817: observation of gravitational waves from a binary neutron star inspiral. *Phys. Rev. Lett.* **119**, 161101 (2017).
24. Wanajo, S. et al. Production of all the r-process nuclides in the dynamical ejecta of neutron star mergers. *Astrophys. J.* **789**, L39 (2014).
25. Janka, H.-T. Explosion mechanisms of core-collapse supernovae. *Annu. Rev. Nucl. Part. Sci.* **62**, 407–451 (2012).
26. Bruenn, S. W. et al. The development of explosions in axisymmetric ab initio core-collapse supernova simulations of 12–25 $M_{\odot}$ stars. *Astrophys. J.* **818**, 123 (2016).
27. MacFadyen, A. I. & Woosley, S. E. Collapsars: gamma-ray bursts and explosions in "failed supernovae". *Astrophys. J.* **524**, 262–289 (1999).
28. Metzger, B. D., Giannios, D., Thompson, T. A., Bucciantini, N. & Quataert, E. The protomagnetar model for gamma-ray bursts. *Mon. Not. R. Astron. Soc.* **413**, 2031–2056 (2011).

Methods

Observational data

SMSS 2003−1142 was identified as a candidate extremely metal-poor ([Fe/H] < −3) star from photometry during the SkyMapper search for extremely metal-poor stars[15]. It was subsequently observed with the WiFeS integral field spectrograph[29] on the Australian National University's 2.3-m telescope at Siding Spring Observatory using the B3000 and R3000 gratings to provide a resolving power of R = 3,000. Comparison of the flux-calibrated spectra against a grid of model fluxes[30] indicated a metallicity of [Fe/H] = −3.75. SMSS 2003−1142 was therefore sufficiently metal-poor to be included in our list for follow-up study at high spectral resolution.

High-resolution spectroscopic observations of SMSS 2003−1142 were obtained using the Magellan Inamori Kyocera Echelle (MIKE) spectrograph[31] at the 6.5-m Magellan telescope on 2017 October 09. The exposure time was 720 s and wavelength coverage from 3,400 Å to 9,000 Å was obtained. The observations were performed using a 1.0-arcsec slit (with 2 × 2 charge-coupled device (CCD) binning), which provided a resolving power of R = 28,000 in the blue arm and R = 22,000 in the red arm. The spectra were reduced using the CARPY pipeline[32]. The signal-to-noise ratio of the reduced spectrum was 86 per 0.045-Å pixel near 4,500 Å.

From our analysis of the MIKE spectrum, we confirmed the low-metallicity nature of the object, finding [Fe/H] = −3.5, and recognized that the Eu abundance was unusually high, [Eu/Fe] = +1.7 dex. In addition to Fe and Eu, we measured the relative abundances for 25 chemical elements and found enhancements in the [X/Fe] abundance ratios for ten neutron-capture elements from Sr (Z = 38) to Er (Z = 68). To conduct a more detailed chemical abundance analysis, we required additional observations extending to bluer wavelengths at higher spectral resolution and signal-to-noise ratio.

We were awarded Director's Discretionary Time on the European Southern Observatory's (ESO) Very Large Telescope (VLT) using the Ultraviolet and Visual Echelle Spectrograph (UVES[33]) (ESO proposal 2103.D-5062(A)). Six sets of 1,500-s exposures were obtained on 2019 September 06. We selected the 390+580 setting, which provided wavelength coverage from 3,300 Å to 4,500 Å in the blue arm and from 4,800 Å to 6,800 Å in the red arm. We used the 1.0-arcsec slit in the blue (2 × 2 CCD binning) and the 0.3-arcsec slit in the red (1 × 1 CCD binning), which provided spectral resolutions of R = 40,000 and R = 110,000 in the blue and red arms, respectively. The data were reduced using the ESO Reflex environment and UVES pipeline version 5.10.4. In the co-added spectra, the signal-to-noise ratio near 3,400 Å was 100 per re-binned 0.027-Å pixel. Our analysis focused on the spectra from the blue arm.

Stellar parameters and abundance determination

Stellar parameters were obtained using previous methods[34,35]. In brief, the effective temperature was determined from fitting model atmosphere fluxes to the spectrophotometric observations from the Australian National University's 2.3-m telescope. The surface gravity was adopted from isochrones assuming the effective temperature and an age of 10 Gyr. Dwarf–giant discrimination was obtained from the WiFeS spectrophotometric observations; confirmation of the giant evolutionary state was provided by Gaia EDR3[36], where the parallax indicates an absolute magnitude in G of −0.4. We report an effective temperature of $T_{\rm eff}$ = 5,175 K, a surface gravity of log(g) = 2.44 (cgs), a microturbulent velocity of 1.9 km s^{-1} and a metallicity of [Fe/H] = −3.5.

Element abundances were obtained from equivalent-width measurements or spectrum synthesis[37], using the stellar line analysis program MOOG[38,39] and one-dimensional local thermodynamic equilibrium (LTE) model atmospheres[40]. Extended Data Fig. 1 illustrates an example spectrum synthesis fit to Zn and Eu lines. Uncertainties in the stellar parameters were estimated to be ±100 K for effective temperature, ±0.3 for surface gravity, ±0.3 km s^{-1} for microturbulent velocity and ±0.1 dex for metallicity; element abundance uncertainties were obtained using standard procedures[37], with the uncertainties in the abundances added in quadrature.

The [X/Fe] ratios were computed using the following approach. For neutral species (for example, Na I and Mg I), we used the Fe abundance as determined from the neutral Fe lines, so the ratios are [Na I /Fe I], [Mg I/Fe I], and so on. For the singly ionized species (for example, Ti II and Sr II), we used the Fe abundance from the singly ionized iron lines, for example, [Ti II/Fe II] and [Sr II/Fe II].

Non-LTE abundance corrections were computed for Na, Mg, Al, Si, Ca, Mn, Fe and Ba. When using all elements (excluding N, Na, Sc, Ti and upper limits) and including those non-LTE abundance corrections, the root-mean-square (RMS) values for the magnetorotational hypernova and neutron-star merger models are 0.44 dex and 0.46 dex, respectively. (For comparison, the LTE RMS values are 0.44 dex and 0.47 dex for the magnetorotational hypernova and neutron-star merger models, respectively.) Therefore, the magnetorotational hypernova model is still preferred over the neutron-star merger model even when taking into account non-LTE abundance corrections where available.

The evolutionary correction for the C abundance[41] is only 0.01 dex. Therefore, we may essentially ignore any evolutionary mixing effects that potentially could decrease the C and raise the N surface abundances.

In Extended Data Fig. 2, we compare the relative abundances for C, N, Zn, Ba, Eu and Th for a subset of highly r-process-enhanced objects and for other metal-poor stars[18]. SMSS 2003−1142 has the highest [(Zn,Ba,Eu,Th)/Fe] ratios, and high [N/Fe] ratio, when compared to the other stars, which illustrates its unique nature. Among the r-process-enhanced metal-poor stars, some exhibit detectable amounts of the radioactive elements Th and/or U[17]. Comparison of those abundances with the scaled solar r-process element pattern enables nucleo-chronometric age dating[17]. However, for a subset of these objects, the Th and/or U abundances are higher than the scaled solar values, which would imply a negative age. These stars are referred to as actinide boost stars. Although SMSS 2003−1142 is the most iron-poor of the actinide boost stars, it differs from other such objects in the [Th/Fe] versus [Zn/Fe] plane; specifically, SMSS 2003−1142 has higher ratios for both Th and Zn by 0.2 dex. Moreover, when compared to stable r-process-element abundances, the age for SMSS 2003−1142 inferred from the radioactive decay of Th and U is extremely uncertain, with estimates ranging from −11 Gyr to +11 Gyr.

Kinematics

SMSS 2003−1142 is also known as Gaia DR2 4190620966764303488. Independent studies suggest that this star has typical kinematics for the Milky Way halo population, albeit with a retrograde orbit[42,43]. The radial velocities from the MIKE spectrum, UVES spectrum and Gaia DR2 are in good agreement: −50.7 km s^{-1}, −51.2 km s^{-1} and −52.2 km s^{-1}, respectively.

Theoretical modelling

In Fig. 2, we show the nucleosynthesis yields from a zero-metallicity $25M_{\odot}$ magnetorotational hypernova model. There is no direct observation of such a supernova, and no successful explosion simulation either[44–46]. Consequently, there are no self-consistent nucleosynthesis yields available in the literature. Here we propose a hypernova-like core-collapse explosion associated with the ejection of neutron-rich matter. The ejection of neutron-rich matter from a massive star driven by stellar rotation and magnetic fields has previously been modelled in numerical simulations. We take the nucleosynthesis yields up to U (Z = 1–92) from a post-processing nucleosynthesis calculation[20] (model B11β1.00) of a two-dimensional special-relativistic magnetohydrodynamic simulation[47] for an Fe core from a rotating $25M_{\odot}$ star with solar metallicity (the only metallicity available; the nucleosynthesis does not depend on the initial metallicity, but it affects the mass of the Fe

core). Because of the simulation setting, it is not known how much envelope outside the Fe core is ejected into the interstellar medium and how much material falls back onto the central black hole during the explosion. We therefore produced hypothetical nucleosynthetic yields for the whole star, including the envelope. We choose a $25M_{\odot}$ hypernova model, with an explosion energy of 10^{52} erg, no rotation and zero metallicity, from an existing set of supernova–hypernova models that are able to explain the observed abundances in extremely metal-poor stars[48]. The model includes the nucleosynthesis yields up to Ge ($Z = 32$). It produces $0.017M_{\odot}$ of Fe, which is 12 times larger than in the original simulation of a magnetorotational supernova, and is more luminous. The relative contribution (mass) of the neutron-rich ejecta in our magnetorotational hypernova model is determined by matching the observed [Eu/Fe] ratio; it is $0.00035M_{\odot}$, only 1.6% of the ejected matter in the magnetorotational supernova simulation. Finally, we assume that our magnetorotational hypernova exploded into a pristine interstellar medium, from which this extremely metal-poor star was born; the ejecta are diluted into $3 \times 10^4 M_{\odot}$ of primordial gas (H, He and trace amounts of Li), to generate a metallicity of [Fe/H] = −3.5.

The progenitor star does not have to be $25M_{\odot}$. It is possible to reproduce the observed abundance pattern with a $40M_{\odot}$ hypernova (3×10^{52} erg), which ejects $0.33M_{\odot}$ of Fe, associated with the ejection of $0.007M_{\odot}$ of neutron-rich matter and diluted into $6 \times 10^5 M_{\odot}$ of primordial gas. A $15M_{\odot}$ supernova (10^{51} erg) could also reproduce the observed [Mg/Fe] ratio, but would result in lower [(Ca,Co,Zn)/Fe] ratios than observed. The observed [Ni/Fe] abundance supports hypernova models over supernova models because the jet explosion can eject Ni that formed near the black hole. Therefore, we conclude that the enrichment source is a $25M_{\odot}$–$40M_{\odot}$ zero-metallicity star.

A magnetorotational hypernova is a jet explosion triggered by magnetic fields and core rotation, associated with ejection of neutron-rich matter, as shown in magnetohydrodynamic simulations[4,20,49]. However, the ejected Fe mass in our model is larger than in the simulations. Hence, our magnetorotational hypernova is more luminous (a few magnitudes brighter) than the theoretical magnetorotational supernova (and several magnitudes brighter than a kilonova), but can be fainter or brighter than the supernovae observed in the nearby Universe. Magnetorotational hypernova may also be related to long-duration γ-ray bursts and/or super-luminous supernovae. The central engine may be similar to those in collapsar[27] or magnetar[28] models. Currently, neither yields nor base explosion simulations are available, as both require three-dimensional hydrodynamical simulations that include general relativity and magnetic fields. The discovery and analysis of SMSS 2003–1142 will hopefully stimulate further study of magnetorotational hypernova.

Production of neutron-capture elements by the explosion of a massive rotating star has also been suggested as one of the possible explanations of the abundance distribution in the r-process-rich star RAVE J183013.5−455510[50]. However, that object has considerably different abundances compared to SMSS 2003–1142; for example, SMSS 2003–1142 has much lower C and higher Eu and Th abundances. As for alternative possibilities, it is not possible to explain the Th abundances with a spin star model[51]. It may be possible that SMSS 2003–1142 was enriched by multiple population III supernovae; this possibility has been discussed in relation to the multiplicity of the first stars[52]. However, with multiple enrichment events it would be difficult to explain the low [Fe/H] ratio of normal-C-abundance stars such as SMSS 2003–1142.

Figure 2 also shows an alternative model that involves a neutron-star merger. Neutron stars form after supernova explosions of massive stars (greater than $8M_{\odot}$)[8], and binary systems of two neutron stars are observed. Nevertheless, it takes a finite amount of time for two neutron stars to merge, the so-called delay time. There are various binary population synthesis calculations that predict the distribution of the delay times[53–55]. Therefore, it is likely that chemical enrichment has occurred before the first neutron-star mergers. Consequently, for the background interstellar medium, we take the elemental abundances from a Galactic chemical evolution model[18], where [Fe/H] reaches about −3.5 at $t \approx 60$ Myr, where t denotes the time after the onset of star formation. This is before type Ia supernovae start to occur. Asymptotic giant-branch stars and electron-capture supernovae, both of which could produce some neutron-capture elements, do not contribute either at such an early time. We add the enrichment from a neutron-star merger to the background composition of the interstellar medium. We use post-processing nucleosynthesis yields from a three-dimensional general-relativistic simulation involving a merger of two $1.3M_{\odot}$ neutron stars[24]. The ejecta mass of the simulation is $0.01M_{\odot}$, which is mixed into $3 \times 10^8 M_{\odot}$ of the slightly enriched interstellar medium (with [Fe/H] ≈ −3.5) to match the observed [Eu/Fe] ratio, before the formation of SMSS 2003–1142.

There are two crucial problems in this neutron-star merger scenario, the rate and the delay time. The adopted Galactic chemical evolution model self-consistently includes chemical enrichment from all stellar masses from $0.01M_{\odot}$ to $50M_{\odot}$, assuming the Kroupa initial mass function (hypernovae are not included). The star-formation history is constrained to match the observed metallicity distribution function of stars in the solar neighbourhood. In the model, the metallicity of the interstellar medium reaches [Fe/H] ≈ −3.5 at $t \approx 60$ Myr. At this time, not many stars have formed, so the number of double neutron-star systems is extremely small. Moreover, the timescale is too short compared with the typical delay time of neutron-star mergers, which is about 100 Myr[53–55] or longer (the delay-time distribution depends on the parameters of the binary population synthesis). In a similar model for the Galactic halo[18], chemical enrichment takes place quickly but inefficiently; although the number of double neutron-star systems is slightly larger, the [Fe/H] ratio reaches about −3.5 at $t = 10$ Myr, which makes it even harder to have a neutron-star merger. Alternatively, it is possible to have interstellar matter that is locally less enriched compared with the Galactic average at a given time. This inhomogeneous enrichment may be important for dwarf satellite galaxies, and in a Galactic chemical evolution model for ultrafaint dwarf galaxies the [Fe/H] ratio could stay below −3.5 at $t = 300$ Myr. This effect should be studied with more self-consistent hydrodynamical simulations, although the frequency of the enrichment from neutron-star mergers at [Fe/H] ≈ −3.5 was found to be extremely low in simulations of a Milky Way-type galaxy[5,56].

The detailed abundance pattern above Ge ($Z = 32$) depends on the parameters in the r-process calculations, such as the strength of rotation and magnetic field for magnetorotational supernova[20,49], the mass and equation of state of neutron stars[24,57], the detailed modelling of neutrino transport[45] and nuclear fissions, and nuclear reaction rates. We find in the magnetorotational supernova model that the elements around $A \approx 90$ are overproduced whereas the elements around $A \approx 140$ are underproduced, which may suggest a possible problem with fission modelling. The other effects can change the resultant distribution of the electron fraction (Y_e) in the simulations. Matter with $Y_e < 0.5$ is neutron-rich, and lower values of Y_e tend to produce heavier elements. The high abundances of Th and U are caused by matter with $Y_e < 0.1$ in the adopted magnetorotational supernova simulation, but are not reproduced in the adopted neutron-star merger simulation. The relatively high abundances of the second (Ba) peak elements are caused by the matter with $Y_e \approx 0.2$ in the neutron-star merger simulation. These elements are underproduced in the magnetorotational supernova simulation, but could be increased with different parameters and/or in future self-consistent three-dimensional, magnetohydrodynamic, general-relativistic simulations. Alternatively, the Ba abundance might be enhanced by stellar rotation[51], but this would result in even higher [(Sr,Y,Zr)/Fe] ratios than in the models presented in Fig. 2, and hence is not a preferred solution.

Finally, following previous work[12], when computing the RMS values provided in the caption for Fig. 2, we excluded N and Na because

the model does not include stellar rotation. We also exclude Sc and Ti because these elements are underproduced in one-dimensional supernova models[12]. We also exclude the elements from Ba to Nd, inclusive, because of the uncertainties discussed above. Regardless of whether we use our preferred set of elements ($Z < 56$ and $Z > 60$ and excluding N, Na, Sc and Ti) or all elements (excluding N, Na, Sc and Ti), the RMS values favour the magnetorotational hypernova model over the neutron-star merger model.

Data availability

The data used in this study are available in the ESO archive (https://archive.eso.org/eso/eso_archive_main.html) under program ID 2103.D-5062(A).

Code availability

The stellar line analysis program MOOG is available at https://www.as.utexas.edu/~chris/moog.html. The stellar model atmospheres are available at http://kurucz.harvard.edu/grids.html.

29. Dopita, M. et al. The Wide Field Spectrograph (WiFeS): performance and data reduction. *Astrophys. Space Sci.* **327**, 245–257 (2010).
30. Gustafsson, B. et al. A grid of MARCS model atmospheres for late-type stars. I. Methods and general properties. *Astron. Astrophys.* **486**, 951–970 (2008).
31. Bernstein, R., Shectman, S. A., Gunnels, S. M., Mochnacki, S. & Athey, A. E. MIKE: a double echelle spectrograph for the Magellan telescopes at Las Campanas Observatory. *Proc. SPIE* **4841**, 1694–1704 (2003).
32. Kelson, D. D. Optimal techniques in two-dimensional spectroscopy: background subtraction for the 21st century. *Publ. Astron. Soc. Pacif.* **115**, 688–699 (2003).
33. Dekker, H., D'Odorico, S., Kaufer, A., Delabre, B. & Kotzlowski, H. Design, construction, and performance of UVES, the echelle spectrograph for the UT2 Kueyen Telescope at the ESO Paranal. *Proc. SPIE* **4008**, 534–545 (2000).
34. Norris, J. et al. The most metal-poor stars. I. Discovery, data, and atmospheric parameters. *Astrophys. J.* **762**, 25 (2013).
35. Yong, D. et al. The most metal-poor stars. II. Chemical abundances of 190 metal-poor stars including 10 new stars with [Fe/H] ≤ −3.5. *Astrophys. J.* **762**, 26 (2013).
36. Gaia Collaboration. Gaia early data release 3: summary of the contents and survey properties. *Astron. Astrophys.* **469**, A1 (2021).
37. Yong, D. et al. A chemical signature from fast-rotating low-metallicity massive stars: ROA 276 in ω Centauri. *Astrophys. J.* **837**, 176 (2017).
38. Sneden, C. The nitrogen abundance of the very metal-poor star HD 122563. *Astrophys. J.* **184**, 839–849 (1973).
39. Sobeck, J. et al. The abundances of neutron-capture species in the very metal-poor globular cluster M15: a uniform analysis of red giant branch and red horizontal branch stars. *Astron. J.* **141**, 175 (2011).
40. Castelli, F. & Kurucz, R. L. New grids of ATLAS9 model atmospheres. In *Proc. IAU Symp. No. 210 Modelling of Stellar Atmospheres* (eds Piskunov, N. et al.) poster A20 (2003).
41. Placco, V. et al. Carbon-enhanced metal-poor star frequencies in the Galaxy: corrections for the effect of evolutionary status on carbon abundances. *Astrophys. J.* **797**, 21 (2014).
42. Mackereth, J. T. & Bovy, J. Fast estimation of orbital parameters in Milky Way-like potentials. *Publ. Astron. Soc. Pacif.* **130**, 114501 (2018).
43. Cordoni, G. et al. Exploring the Galaxy's halo and very metal-weak thick disk with SkyMapper and Gaia DR2. *Mon. Not. R. Astron. Soc.* **503**, 2539–2561 (2021).
44. Mösta, P. et al. Magnetorotational core-collapse supernovae in three dimensions. *Astrophys. J.* **785**, L29 (2014).
45. Kuroda, T., Arcones, A., Takiwaki, T. & Kotake, K. Magnetorotational explosion of a massive star supported by neutrino heating in general relativistic three-dimensional simulations. *Astrophys. J.* **896**, 102 (2020).
46. Obergaulinger, M. & Aloy, M.-A. Magnetorotational core collapse of possible GRB progenitors. III. Three-dimensional models. *Mon. Not. R. Astron. Soc.* **503**, 4942–4963 (2021).
47. Takiwaki, T., Kotake, K. & Sato, K. Special relativistic simulations of magnetically dominated jets in collapsing massive stars. *Astrophys. J.* **691**, 1360 (2009).
48. Kobayashi, C., Ishigaki, M. N., Tominaga, N. & Nomoto, K. The origin of low [α/Fe] ratios in extremely metal-poor stars. *Astrophys. J.* **785**, L5 (2014).
49. Reichert, M., Obergaulinger, M., Eichler, M., Aloy, M. A. & Arcones, A. Nucleosynthesis in magneto-rotational supernovae. *Mon. Not. R. Astron. Soc.* **501**, 5733–5745 (2021).
50. Placco, V. et al. The r-process alliance: the peculiar chemical abundance pattern of RAVE J183013.5−455510. *Astrophys. J.* **897**, 78 (2020).
51. Choplin, A., Tominaga, N. & Meyer, B. S. A strong neutron burst in jet-like supernovae of spinstars. *Astron. Astrophys.* **639**, A126 (2020).
52. Skinner, D. & Wise, J. H. Cradles of the first stars: self-shielding, halo masses, and multiplicity. *Mon. Not. R. Astron. Soc.* **492**, 4386–4397 (2020).
53. Mennekens, N. & Vanbeveren, D. Massive double compact object mergers: gravitational wave sources and r-process element production sites. *Astron. Astrophys.* **564**, A134 (2014).
54. Belczynski, K. et al. The origin of the first neutron star–neutron star merger. *Astron. Astrophys.* **615**, A91 (2018).
55. Vigna-Gómez, A. et al. On the formation history of Galactic double neutron stars. *Mon. Not. R. Astron. Soc.* **481**, 4009–4029 (2018).
56. van de Voort, F. et al. Neutron star mergers and rare core-collapse supernovae as sources of r-process enrichment in simulated galaxies. *Mon. Not. R. Astron. Soc.* **494**, 4867–4883 (2020).
57. Goriely, S., Bauswein, A. & Janka, H.-T. r-process nucleosynthesis in dynamically ejected matter of neutron star mergers. *Astrophys. J.* **738**, L32 (2011).

Acknowledgements This paper includes data gathered with the 6.5-m Magellan Telescopes located at Las Campanas Observatory, Chile, and is based on observations collected at the European Southern Observatory under ESO programme DDT 2103.D-5062(A). This research was supported by the Australian Research Council Centre of Excellence for All Sky Astrophysics in 3 Dimensions (ASTRO 3D), through project number CE170100013. C.K. acknowledges funding from the UK Science and Technology Facility Council (STFC) through grant ST/M000958/1 and ST/ R000905/1, and the Stromlo Distinguished Visitor Program at ANU. K.L. acknowledges funds from the European Research Council (ERC) under the European Union's Horizon 2020 research and innovation programme (grant agreement number 852977). A.F.M. acknowledges support from the European Union's Horizon 2020 research and innovation programme under Marie Sklodowska-Curie grant agreement number 797100. A.R.C. acknowledges Australian Research Council grant DE190100656.

Author contributions G.S.D.C., M.S.B., M.A., A.D.M., A.F.M., S.J.M. and T.N. were involved in the target selection and low-resolution spectroscopic observation campaigns. D.Y., G.S.D.C., A.C., A.F. and T.N. were involved in the high-resolution spectroscopic observations. K.L. and T.N. computed the non-LTE corrections. The manuscript was written by D.Y., C.K. and G.S.D.C., with contributions from all authors.

Competing interests The authors declare no competing interests.

Additional information

Supplementary information The online version contains supplementary material available at https://doi.org/10.1038/s41586-021-03611-2.

Correspondence and requests for materials should be addressed to D.Y.

Peer review information *Nature* thanks Timothy Beers and Kim Venn for their contribution to the peer review of this work. Peer reviewer reports are available.

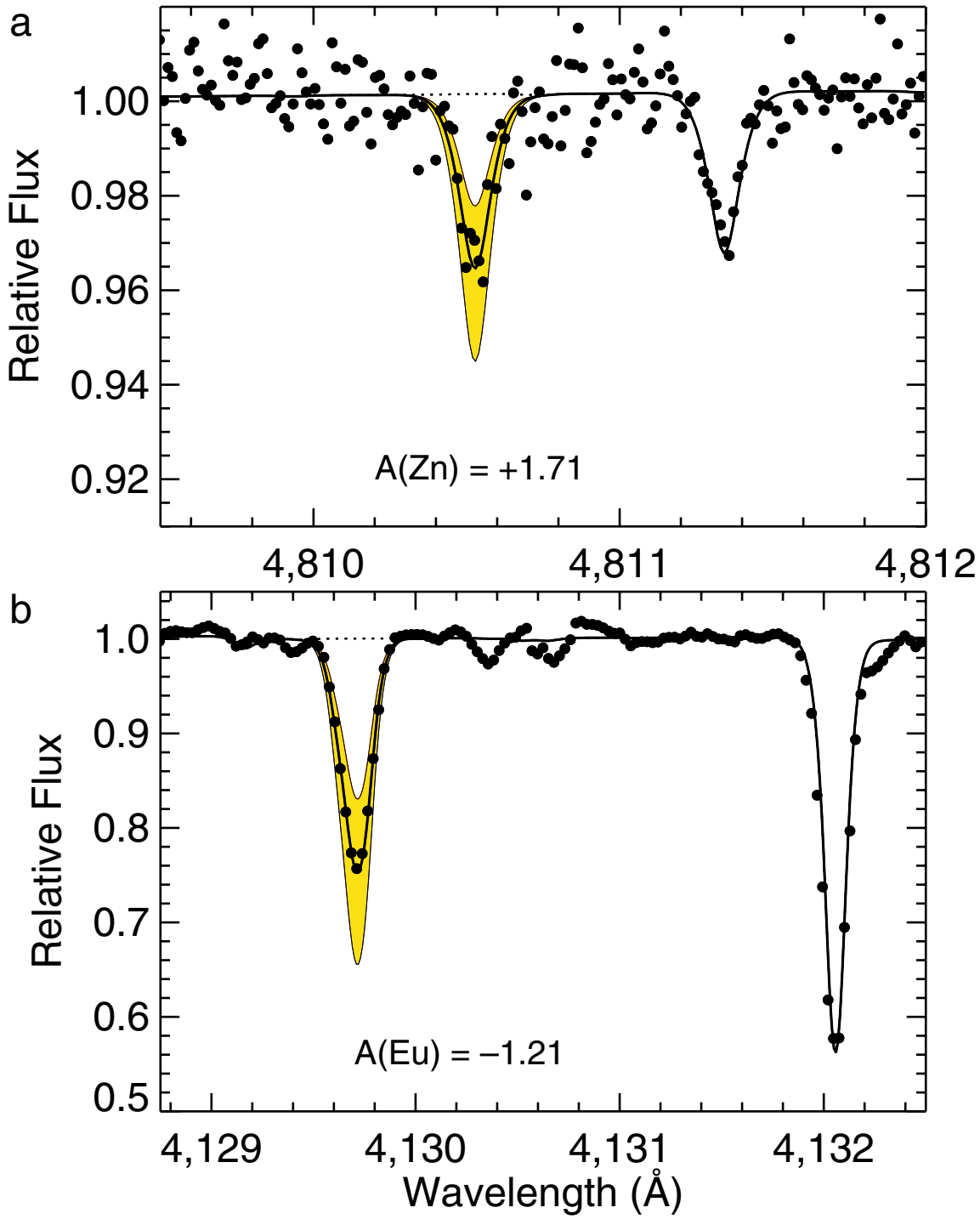

Extended Data Fig. 1 | Spectrum of SMSS 2003−1142. a, **b**, Spectrum synthesis fit to the 4,810-Å Zn I line (**a**) and the 4,129-Å Eu II line (**b**). The observed spectra are shown as small circles, the best-fitting synthetic spectrum is shown as the solid black line and the yellow region indicates ±0.2 dex from the best fit.

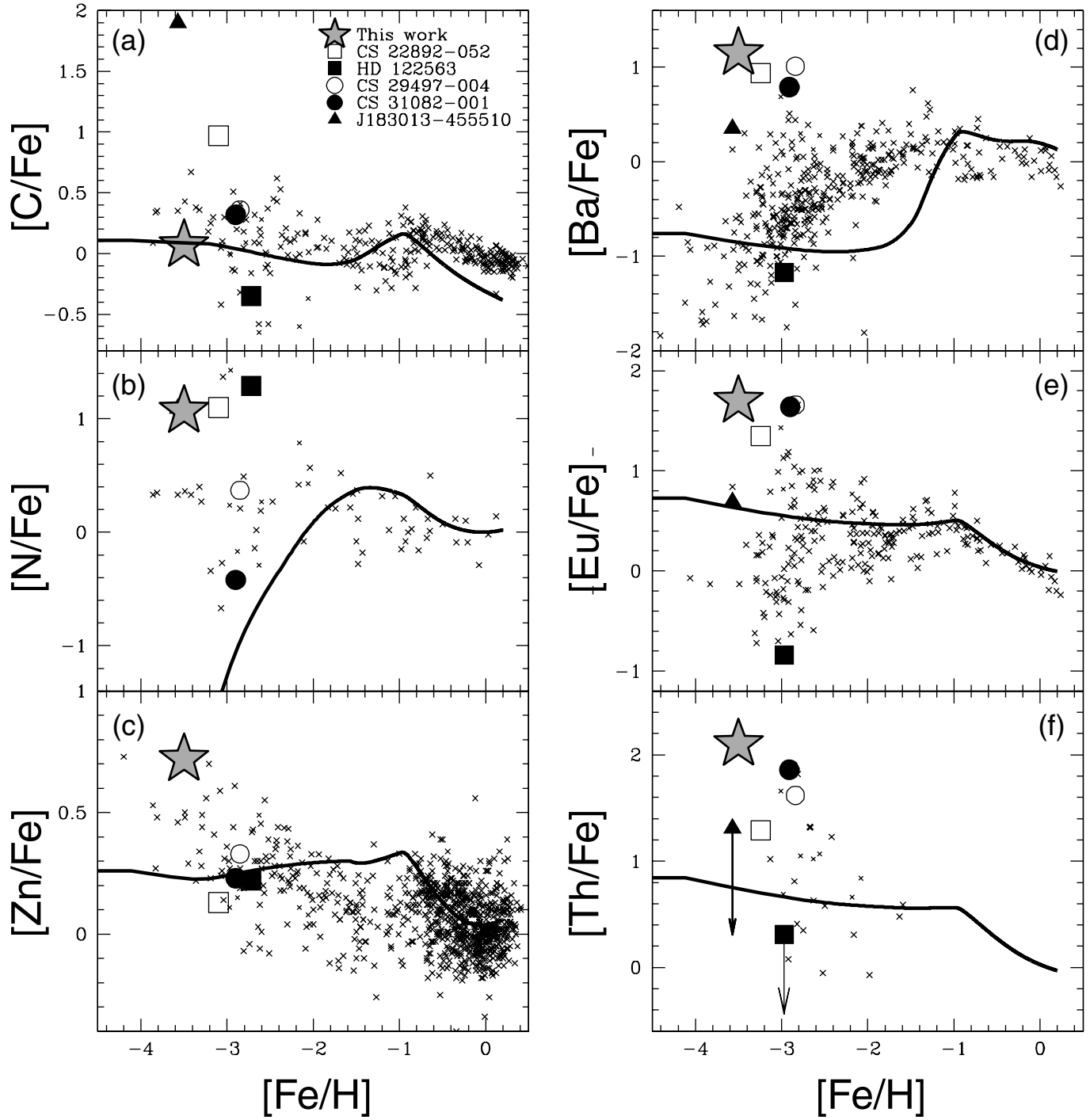

Extended Data Fig. 2 | Abundance ratios in halo stars. a–f, Element to Fe ratios, [X/Fe], as a function of metallicity, [Fe/H], based on literature data[20] (small crosses), for C (**a**), N (**b**), Zn (**c**), Ba (**d**), Eu (**e**) and Th (**f**). The lines are the Galactic chemical evolution model predictions for the solar neighbourhood[20]. SMSS 2003−1142 is shown as the large five-pointed star. The locations of well-studied r-process-rich stars (CS 22892−052, HD 122563, CS 29497−004, CS 31082−001 and RAVE J183013.5−455510) are highlighted by large symbols. Arrow indicate upper limits.